THE CATHOLIC UNIVERSITY OF AMERICA
DEPARTMENT OF ELECTRICAL ENGINEERING

LEARNING-BASED POSITION CONTROL OF A CLOSED-KINEMATIC CHAIN ROBOT END-EFFECTOR

Charles C. Nguyen
Principal Investigator and Associate Professor
and
Zhen-Lei Zhou
Graduate Research Assistant

NAG 5-780

submitted to
Dr. Charles E. Campbell
Code 735.1
Goddard Space Flight Center (NASA)
Greenbelt, Maryland

February 1990

SUMMARY

This report present the research results obtained from the research grant entitled "Active Control of Robot Manipulator Compliance," funded by the Goddard Space Flight Center (NASA) under the Grant Number NAG 5-780, for the period between August 1st, 1989 and February 1st, 1990.

*In this report, we present a trajectory control scheme whose design is based on learning theory, for a six-degree-of-freedom (***DOF***) robot end-effector built to study robotic assembly of NASA hardwares in space. The control scheme consists of two control systems: the feedback control system and the learning control system. The feedback control system is designed using the concept of linearization about a selected operating point, and the method of pole placement so that the closed-loop linearized system is stabilized. The learning control scheme consisting of PD-type learning controllers, provides additional inputs to improve the end-effector performance after each trial. Experimental studies performed on a 2 DOF end-effector built at CUA, for 3 tracking cases show that actual trajectories approach desired trajectories as the number of trials increases. In fact, the tracking errors are substantially reduced only after 5 trials.*

1 INTRODUCTION

Repeatable tasks in a factory or in space can be performed by a robot manipulator that is taught off-line via a so-called *teaching and playback scheme* or by a manipulator that is equipped with an on-line learning ability produced by a *self learning control scheme* without human supervision. Learning control theory which was originated from the concept suggesting that robot manipulators like human beings can learn from measurement data of previous operations in order to improve their performance in future operations, has attracted control researchers' attention since many years [1] and recently has been considered for control of robot manipulators [2]-[10]. Control of mechanical arms using learning control theory was considered by Uchiyama [2] who proposed one of the first learning control schemes to be applied to robotics. Realizing that it is difficult to obtain full descriptions of robot manipulator dynamics due to their unknown characteristics such as friction, backlash, and non-rigidity, etc, Arimoto and his co-workers [3] developed a so-called *Betterment Process* to provide manipulators with a learning ability. The betterment process is based on a simple iteration rule that generates a current actuator input which is better than the previous one under the condition that a desired output is specified. Applications of the betterment process to linear time-invariant systems and to a class of nonlinear systems are presented in [4]. The concept of betterment process was further developed and applied into a learning-based position/force control scheme [5] which was experimentally shown to be very effective in polishing a curved object. Based on the principle of the betterment process, three types of learning control schemes were proposed by Arimoto and others in the work presented in [6] which also addressed the convergence problem of the proposed schemes. The synthesis of repetitive control systems for a subclass of systems whose outputs are controlled to follow periodic reference commands was considered by Hara and his co-workers [7]. Relaxing the rank condition imposed by Arimoto's learning control scheme [3] and using state variable errors, Togai and Yamano [8] introduced a discrete learning algorithm to control discrete systems performing repetitive operations. They show that the discrete approach is generally more advantageous than the analog approach used in [3]-[6]. Based on explicit modeling of robot manipulators and using inverse manipulator model, Atkeson and McIntyre [9] proposed a learning algorithm to reduce trajectory following errors of repetitive robot motions. Nguyen and others [10] combined the concepts of hybrid control and learning control to design a learning-based hybrid control scheme for controlling force and position in part assembly problems.

In this report, we consider the application of learning control theory into Cartesian trajectory control of a 6 DOF robot end-effector built at the Goddard Space Flight Center (NASA) to study telerobotic assembly of NASA hardwares [11]. In particular, a learning-based trajectory control scheme consisting of a feedback control system and a learning control system is presented. The feedback control system ensures that the linearized model of the closed-loop system is stable while the learning system provides additional inputs to the end-effector actuators so that the responses can be improved

after each trial. Using the methods of linearization about a desired pattern and pole placement, we will show that proper selection of the learning control system gains will provide the end-effector with an on-line learning ability so that it can autonomously reduce its errors as the number of trials increases. The performance of the developed learning control scheme will be investigated experimentally on a 2 DOF end-effector and investigation results will be discussed.

2 THE ROBOT END-EFFECTOR

Recently a 6 DOF end-effector was designed and built at NASA/Goddard Space Flight Center to serve as a testbed for studying the feasibility of autonomous assembly of parts in a telerobotic operation in space. As illustrated in Figure 1, the end-effector resembles the structure of a Stewart platform [13], and mainly consists of a payload platform, a base platform, six linear actuators and a gripper. The upper movable payload platform is coupled to the base platform by six axially extensible rods and recirculating ballscrews driven by dc motors are used to provide the extensibility. The motion of the upper payload platform is produced by the combination of extending and shortening the actuator lengths. Each end of the actuator links is mounted to the platforms by 2 rotary joints with intersecting and perpendicular axes. Solutions of forward and inverse kinematic problems and equations of motion of the above end-effector can be found in [11]-[12].

3 THE LEARNING CONTROL SCHEME

Figure 2 presents the learning-based control scheme proposed to control the motion of the end-effector presented in previous section. The control scheme mainly consists of 2 systems: the feedback control system and the learning control system. The feedback control system improves the end-effector dynamics in terms of system stability and tracking quality and the learning control system reduces the transient and steady-state errors of the end-effector responses after each trial.

In the feedback control system, linear voltage differential transformers (**LVDT**) serving as position sensors are mounted along the end-effector actuators to measure their lengths l_i for i=1,2,...,6, compactly represented by the joint position vector $\mathbf{l}$ which is then compared with the desired joint position vector $\mathbf{l}_d$ to generate the joint error vector $\mathbf{l}_e$. Since closed-form solutions exist for the inverse kinematic problem of a closed-kinematic chain mechanism [11], inverse kinematics is employed in the above control scheme to transform desired Cartesian position[1] vector $\mathbf{x}_d$ into the corresponding desired joint position corresponding $\mathbf{l}_d$. The joint errors will then serve as the inputs to the feedback controller whose gains are designed such that the end-effector tracks a set of desired Cartesian position trajectories with minimum settling time and minimum

[1] In this report, Cartesian position implies both position and orientation.

steady-state errors. Here settling time is defined as the time the controller would need to track the actual response to reach about 5 percent of the deviation between the desired and actual time trajectories. Steady-state error denotes the constant deviation between the desired and actual spatial Cartesian paths after the response has settled. In [14], linearization and pole placement methods were employed to design the controller gains and satisfactory results were obtained. The tracking performance of the end-effector was further improved in [15] where the controller gains were designed using the concepts of model reference adaptive control and Lyapunov theory. Simulation results showed that although the responses were substantially improved in [15], there were still some minor difference between the desired and actual responses due to dynamic interferences caused by the nonlinearity of the end-effector dynamics. For tasks that are repetitive, the transient and steady-state responses can be further reduced by equipping the end-effector with a learning ability realized by a learning control system that can "learn" from the joint position errors during a trial and provide additional signals to improve the end-effector performance during the next trial.

Figure 3 illustrates the structure of the learning control system that mainly consists of a PD-type learning controller and a large-scale integrated random access memory (**LSI RAM**). The learning process is described in the following scheme:

$$\mathbf{u}_{k+1} = \mathbf{u}_k + \mathbf{\Phi}(\alpha \mathbf{l}_e + \beta \dot{\mathbf{l}}_e) \tag{1}$$

where $\mathbf{u}_k$ denotes the output of the learning control system during the kth trial, $\mathbf{\Phi}$ is a positive definite matrix, α and β are non-negative scalars and

$$\mathbf{l}_e = \mathbf{l}_d - \mathbf{l}. \tag{2}$$

During the kth trial, the information of $\mathbf{u}_{k+1}$ is computed using (1) and stored in the lower part of the RAM as a set of densely sampled digital data. After the kth trial, the stored data will be loaded to the upper part of the memory and will be sent to the actuators during the (k+1)th trial. The lower part of the memory is now empty and ready to store new data. During the kth trial, the input to the end-effector actuators is composed of signals coming from the feedback controller, τ_p, the learning controller, $\mathbf{u}_k$ and an auxiliary signal τ_a, namely

$$\tau_k = \tau_p + \mathbf{u}_k + \tau_a. \tag{3}$$

The auxiliary signal τ_a is included in (3) to compensate the end-effector dynamics as seen later in the design of the controller gains.

4 CONTROL SCHEME DESIGN

Design of the proposed control scheme is performed in three steps: a) linearizing the end-effector dynamics about $\mathbf{l}_d$, b) selecting the controller gains for the feedback control

system so that the linearized closed-loop control system is stable, and c) selecting the controller gains for the learning control system so that the difference between the desired and actual response converges to zero as the number of trials increases to infinity.

The dynamical equations of the end-effector are given by [12]

$$\mathbf{M}(\mathbf{l})\ddot{\mathbf{l}}(t) + \mathbf{N}(\mathbf{l},\dot{\mathbf{l}}) + \mathbf{G}(\mathbf{l}) = \tau(t) \tag{4}$$

where $\mathbf{l}$ denotes the (6x1) joint variable vector containing the length l_i as its ith row, for i=1,2,...,6, $\mathbf{M}(\mathbf{l})$, $\mathbf{N}(\mathbf{l},\dot{\mathbf{l}})$ and $\mathbf{G}(\mathbf{l})$ represent the (6x6) end-effector mass matrix, the (6x1) centrifugal and Coriolis force vector, and the (6x1) gravitational force vector, respectively.

Linearizing (4) about $\mathbf{l}_d$, the desired joint variable vector which corresponds to the Cartesian variable vector $\mathbf{x}_d$ by using Taylor series expansion and neglecting higher order terms, we obtain

$$\mathbf{M}(t)\ddot{\mathbf{z}}(t) + \mathbf{N}(t)\dot{\mathbf{z}}(t) + \mathbf{G}(t)\mathbf{z}(t) + \tau_d(t) = \tau(t) \tag{5}$$

where

$$\mathbf{z}(t) = \mathbf{l}(t) - \mathbf{l}_d(t) \tag{6}$$

$$\mathbf{M}(t) = \mathbf{M}(\mathbf{l}_d) \tag{7}$$

$$\mathbf{N}(t) = \frac{\partial}{\partial \mathbf{l}}\left[\mathbf{N}(\mathbf{l},\dot{\mathbf{l}})\right]_{\mathbf{l}_d,\dot{\mathbf{l}}_d} \tag{8}$$

$$\mathbf{G}(t) = \frac{\partial}{\partial \mathbf{l}}\left[\mathbf{M}(\mathbf{l})\ddot{\mathbf{l}}_d + \mathbf{N}(\mathbf{l},\dot{\mathbf{l}}) + \mathbf{G}(\mathbf{l}_d\right]_{\mathbf{l}_d,\dot{\mathbf{l}}_d} \tag{9}$$

$$\tau_d(t) = \mathbf{M}(\mathbf{l}_d)\ddot{\mathbf{l}}_d(t) + \mathbf{N}(\mathbf{l}_d,\dot{\mathbf{l}}_d) + \mathbf{G}(\mathbf{l}_d). \tag{10}$$

However we have

$$\tau(t) = \tau_p(t) + \mathbf{u}(t) + \tau_a(t) \tag{11}$$

where $\tau_p(t)$, the output of the PD controller of the feedback control system is given by

$$\tau_p(t) = \mathbf{K}_p\mathbf{l}_e + \mathbf{K}_d\dot{\mathbf{l}}_e \tag{12}$$

and $\mathbf{K}_p$ and $\mathbf{K}_d$ are the controller gain matrices of the PD controller.

Now substituting (11)-(12) into (5) yields

$$\mathbf{M}(t)\ddot{\mathbf{z}}(t) + \left[\mathbf{N}(t) + \mathbf{K}_d\right]\dot{\mathbf{z}}(t) + \left[\mathbf{G}(t) + \mathbf{K}_p\right]\mathbf{z}(t) = \mathbf{u}(t) \tag{13}$$

where we let

$$\tau_a(t) = \tau_d(t) \tag{14}$$

and it is noted that

$$\mathbf{l}_e(t) = -\mathbf{z}(t). \tag{15}$$

The system represented by (13) is a linear time-varying control system which can be asymptotically stabilized by properly selecting $\mathbf{K}_p$ and $\mathbf{K}_d$ by using for instance the eigenvalue assignment method in [16].

Using (15), we proceed to rewrite (1) as

$$\mathbf{u}_{k+1}(t) = \mathbf{u}_k(t) - \mathbf{\Phi}\left[\alpha \mathbf{z}_k(t) + \beta \dot{\mathbf{z}}_k(t)\right] \tag{16}$$

where

$$\mathbf{u}_k(t) = \mathbf{M}(t)\ddot{\mathbf{z}}_k(t) + \left[\mathbf{N}(t) + \mathbf{K}_d\right]\dot{\mathbf{z}}_k(t) + \left[\mathbf{G}(t) + \mathbf{K}_p\right]\mathbf{z}_k(t). \tag{17}$$

We recall from (6) that $\mathbf{z}(t)$ denotes the error between the actual joint vector $\mathbf{l}(t)$ and the desired joint vector $\mathbf{l}_d(t)$. Therefore, to obtain good tracking quality, $\mathbf{z}_d(t)$, the desired value for $\mathbf{z}(t)$, should be set to 0. In this case, (16) can be further rewritten as

$$\mathbf{u}_{k+1} = \mathbf{u}_k + \mathbf{\Phi}\left[\alpha(\mathbf{z}_d - \mathbf{z}_k) + \beta(\dot{\mathbf{z}}_d - \dot{\mathbf{z}}_k)\right]. \tag{18}$$

Equations (17) and (18) constitute the general learning scheme of the Cartesian trajectory control scheme.

We proceed to present the following lemma:

Lemma 1 *Consider a class of n-dimensional linear time-varying systems described by*

$$\mathbf{R}(t)\ddot{\xi}(t) + \mathbf{Q}(t)\dot{\xi}(t) + \mathbf{P}(t)\xi(t) = \eta(t) \tag{19}$$

where $\xi(t)$ and $\eta(t)$ are the $(n \times 1)$ controlled variable vector and the $(n \times 1)$input vector, respectively. $\mathbf{R}(t)$, $\mathbf{Q}(t)$ and $\mathbf{P}(t)$ denote $(n \times n)$ time-varying matrices whose elements are continuously differentiable on [0,T] for some positive constant T and $\mathbf{R}(t)$ is positive definite for all $t \in [0,T]$. A learning scheme is defined by

$$\eta_{k+1} = \eta_k + \mathbf{\Gamma}\left[\alpha(\dot{\xi}_d - \xi_k) + \beta(\dot{\xi}_d - \dot{\xi}_k)\right], \tag{20}$$

$$\mathbf{R}(t)\ddot{\xi}_k(t) + \mathbf{Q}(t)\dot{\xi}_k(t) + \mathbf{P}(t)\xi_k(t) = \eta_k(t) \tag{21}$$

$$\dot{\xi}_k(0) = \dot{\xi}_d(0) \quad \xi_k(0) = \xi_d(0) \tag{22}$$

where α and β are non-negative constant scalars, ξ_d denotes the desired trajectory for ξ_k, and $\mathbf{\Gamma}$ is an $(n \times n)$ positive definite matrix.

If η_1 is continuous, ξ_d is continuously differentiable on [0,T], α and β are selected such that $0 < \alpha, \beta \leq 1$, then ξ_k converges to ξ_d uniformly on [0,T] as $k \to \infty$.

The proof of Lemma 1 can be found in [5]. We now present the main result of this report.

Main Result 1 *Consider the robot end-effector whose dynamical equations and linearized model are given by (4) and (5), respectively. If the desired Cartesian trajectory vector $\mathbf{x}_d$ is continuously differentiable on [0,T], and $\dot{\mathbf{x}}_k(0) = \dot{\mathbf{x}}_d(0)$; $\mathbf{x}_k(0) = \mathbf{x}_d(0)$, then the learning control scheme described in (17) and (18) can be designed so that the difference between $\mathbf{x}_k$ and $\mathbf{x}_d$ converges to 0 as $k \to \infty$.*

Proof: In [12], we showed that closed-form solutions exist for the inverse kinematic problem of closed-kinematic chain mechanism. Therefore from the fact that

$$\mathbf{l}_d = \mathbf{IK}(\mathbf{x}_d), \tag{23}$$

where **IK** denotes the inverse kinematic function of the end-effector, if $\mathbf{x}_d$ is continuously differentiable on [0,T], then so is $\mathbf{l}_d$. In this case, using (7)-(9), we observe that $\mathbf{M}(t)$, $\mathbf{N}(t)$ and $\mathbf{G}(t)$ are also continuously differentiable on [0,T]. Consequently, the matrices in (17) are all continuously differentiable on [0,T]. In addition,

$$\dot{\mathbf{z}}_k(0) = \dot{\mathbf{l}}_k(0) - \dot{\mathbf{l}}_d(0) = 0 = \dot{\mathbf{z}}_d(0) \tag{24}$$

$$\mathbf{z}_k(0) = \mathbf{l}_k(0) - \mathbf{l}_d(0) = 0 = \mathbf{z}_d(0) \tag{25}$$

because

$$\dot{\mathbf{l}}_k(0) = \dot{\mathbf{l}}_d(0); \;\; \mathbf{l}_k(0) = \mathbf{l}_d(0), \tag{26}$$

which are derived from the hypothesis of Main Result. Besides, $\mathbf{M}(t)$ is positive definite on [0,T] because so is $\mathbf{M}(1)$. The system represented by (17) is stabilized and consequently $\mathbf{u}_1(t)$ is continuous on [0,T]. Now comparing (16) and (17) with (20) and (21), respectively, and applying Lemma 1, if we select α and β in (18) such that $0 < \alpha, \beta \leq 1$, then $\mathbf{z}_k(t)$ converges to $\mathbf{z}_d(t) = 0$ uniformly on [0,T] as $k \rightarrow \infty$. In other words, $\mathbf{l}_k(t)$ converges to $\mathbf{l}_d(t)$, or equivalently $\mathbf{x}_k(t)$ converges to $\mathbf{x}_d(t)$ uniformly on [0,T] as $k \rightarrow \infty$. The proof of the main result is completed.

5 EXPERIMENTAL STUDY OF 2 DOF CASE

In this section, the proposed learning-based control scheme is implemented to control the motion of a 2 DOF end-effector showed in Figure 4. The end-effector mainly consists of 2 ball-screw linear actuators driven by dc motors and hung below a stationary platform via pin joints. Position feedback is accomplished by 2 **LVDT**'s mounted along the actuator links. The end-effector is controlled by a personal computer through a data acquisition system consisting of an IBM board, an adapter and a software package called Labtech Notebook. PD controllers, learning controller, inverse kinematics, error computation and joint force computation are implemented by Labtech Notebook. Based on the diagram given in Figure 5, the Cartesian position x and y expressed with respect to a reference coordinate system affixed to the stationary platform are related to the joint positions $\mathbf{l}_1$ and $\mathbf{l}_2$ as follows:

$$x = \frac{l_1^2 - l_2^2 + d^2}{2d} \tag{27}$$

and

$$y = -\frac{\sqrt{4d^2 l_1^2 - (l_1^2 - l_2^2 + d^2)^2}}{2d} \tag{28}$$

where d is the distance between the pin joints hanging the actuators. The Lagrangian approach is applied to derive the following equations of motion:

$$\tau(t) = \mathbf{M}(\mathbf{l},\dot{\mathbf{l}})\,\ddot{\mathbf{l}}(t) + \mathbf{N}(\mathbf{l},\dot{\mathbf{l}})\,\dot{\mathbf{l}}(t) + \mathbf{G}(\mathbf{l},\dot{\mathbf{l}}) \tag{29}$$

where

$$\tau(t) = (\tau_1 \;\; \tau_2)^T; \;\; \mathbf{l} = (l_1 \;\; l_2)^T \tag{30}$$

where τ_i and l_i denote the joint force to and the lenght of the ith actuator for i=1,2, respectively. Also

$$\mathbf{M} = \begin{bmatrix} m_1 & 0 \\ 0 & m_1 \end{bmatrix} \tag{31}$$

$$\mathbf{N} = \begin{bmatrix} 0 & \frac{m_1 l_m (l_2 - l_1)}{3u} \\ \frac{m_1 l_m (l_1 - l_2)}{3u} & 0 \end{bmatrix} \tag{32}$$

$$\mathbf{G} = (G_1 \;\; G_2)^T \tag{33}$$

with

$$G_1 = \frac{\left\{ \begin{array}{l} -mgl_m[2l_1^2 u_1(l_1 + l_2) - l_2 u^2] \\ -m_1 g[2u_1 l_1^2(l_1 l_m + l_2 l_m + 2l_1 l_2) - l_2 l_m u^2] \end{array} \right\}}{4dl_1^2 l_2 u} \tag{34}$$

$$G_2 = \frac{\left\{ \begin{array}{l} -mgl_m[2l_2^2 u_2(l_1 + l_2) - l_1 u^2] \\ -m_1 g[2u_2 l_2^2(l_1 l_m + l_2 l_m + 2l_1 l_2) - l_2 l_m u^2] \end{array} \right\}}{4dl_1^2 l_2 u} \tag{35}$$

and

$$u_1 = l_2^2 - l_1^2 + d^2; \;\; u_2 = l_2^2 - l_1^2 + d^2; \;\; u = \sqrt{4d^2 l_1^2 - u_2}, \tag{36}$$

where m_1 is the mass of the moving part of the link,m the total mass of the link, and l_m the fixed length of the actuators and g the gravitational acceleration.

Experiments were performed to study the performance of the proposed learning control scheme implemented to track the end-effector on three different planar paths. The experimental results are reported below where in study case we let the end-effector repeat the task 5 times.

Case 1: Tracking a Straight Line

The straight line to be followed by the end-effector is specified by $y = -1.5x - 68$ $[in\ cm]$ where $x(t) = 0.6t + 25.4$ $[in\ cm]$ and experimental results for this case are reported in Figures 6a-c. Figures 6a and 6b represent the time responses of the horizontal and vertical errors, respectively with respect to the desired trajectories, of the 1st and 5th trials while Figure 6c represents the actual and desired planar motions at the 5th trial. As the results show, the tracking performance was improved substantially at the 5th trial which brought the maximum horizontal error from 0.87 cm down to 0.35 cm and the maximum vertical error from 0.47 cm down to 0.20 cm.

Case 2: Tracking a Sinusoidal Path

The sinusoidal path to be followed by the end-effector is described by $y = sin(2x - 50) - 83$ $[in\ cm]$ where $x(t) = 0.6t + 25.4$ $[in\ cm]$. Figures 7a-c report the experimental results for this case. Figures 7a and 7b illustrate the time responses of the horizontal and vertical errors, respectively, of the 1st and 5th trials while Figure 6c represents the actual and desired planar motions at the 5th trial. We observe that the tracking performance was improved significantly at the 5th trial which brought the maximum horizontal error from 0.84 cm down to 0.30 cm and the maximum vertical error from 1.14 cm down to 0.5 cm.

Case 3: Tracking a Circular Path

Figure 8a-c present the experimental results of tracking a circular path specified by $(x - 34)^2 + (y + 83)^2 = 16$ $[in\ cm]$ where $x(t) = 5sin\frac{\pi}{10}t$ and $y(t) = 5cos\frac{\pi}{10}t$. The time responses of the horizontal and vertical errors are presented in Figures 8a and 8b, respectively and Figure 8c represents the actual and desired planar motions at the 5th trial. As the results show, the tracking performance was improved substantially at the 5th trial which brought the maximum horizontal error from 1.87 cm down to 0.52 cm and the maximum vertical error from 1.54 cm down to 0.71 cm.

In the above experimental study, the following parameters were used:

- *End-Effector Parameters*: $d = 29inches$; $m_1 = 0.59kg$; $m = 4.5kg$
- *Feedback Control System*: PD controller gains:

$$\mathbf{K}_p = \begin{bmatrix} 22\frac{volt}{in} & 0 \\ 0 & 22\frac{volt}{in} \end{bmatrix};\ \mathbf{K}_d = \begin{bmatrix} 0.7\frac{volt.sec}{in} & 0 \\ 0 & 0.7\frac{volt.sec}{in} \end{bmatrix}$$

- *Learning Control System*:

$$\Phi = \begin{bmatrix} 220 & 0 \\ 0 & 2 \end{bmatrix},$$

$\alpha = \frac{1}{20}$; $\beta = \frac{19}{20}$.

6 CONCLUSION

A learning-based control scheme was proposed in this report to control the Cartesian trajectory of a 6 DOF end-effector performing assembly tasks that are repetitive. The learning control scheme consists of a feedback control system that improves the end-effector dynamics and a learning control system that can "learn" from errors to improve the end-effector performance after each trial. Linearization about a desired trajectory was applied to convert the nonlinear equations of motion of the end-effector into a

linear time-varying system which can be stabilized by properly selecting feedback PD controller gains by using eigenvalue assignment method. We then showed that the learning controller gains can be designed such that the end-effector motion approaches a desired motion in a repeatable assembly task, as the number of trials increases. Experimental studies performed on a 2 DOF end-effector showed that the errors converged as the number of trials increased. In particular, the tracking performance of the end-effector was substantially improved only after 5 trials. Future research activities will be directed to the investigation of the proposed learning control scheme on the 6 DOF end-effector using computer simulation and experimentation. Attention should also be paid to the development of a learning-based control system which consists of an on-line adaptive feedback control system [15] and an off-line learning control system. Implementation of a learning-based control scheme [10] to control position and force of the 6 DOF end-effector should also be investigated experimentally.

References

[1] Fu, K.S., "Learning Control Systems-Review and Outlook," *IEEE Trans. Automatic Control*, AC-15, pp. 210-221, April 1970.

[2] Uchiyama, M., "Formation of High Speed Motion Pattern of Mechanical Arm by Trial," *Transactions, Society of Instrument and Control Engineers*, Vol. 19, No. 5, pp. 706-712, 1978.

[3] Arimoto, S., Kawamura, S., Miyazaki, F., "Bettering Operation of Robots by Learning," *Journal of Robotic Systems*, Vol. 1, No. 2, pp. 123-140, 1984.

[4] Arimoto, S., Kawamura, S., Miyazaki, F., "Bettering Operations of Dynamic Systems by Learning: a new Control Theory for Servomechanism or Mechatronics Systems," *Proc. 23rd Conf. Decision and Control*, pp. 1064-1069, December 1984.

[5] Kawamura, S., Miyazaki, F., Arimoto, S., "Applications of Learning Method for Dynamic Control of Robot Manipulators," *Proc. 24th Conf. Decision and Control*, pp. 1381-1386, December 1985.

[6] Arimoto, S. et al, "Learning Control Theory for Dynamical Systems," *Proc. 24th Conf. Decision and Control*, pp. 1375-1380, December 1985.

[7] Hara, S., Omata, T., Nakano, M., "Synthesis of Repetitive Control Systems and Its Applications," *Proc. 24th Conf. Decision and Control*, pp. 1387-1392, December 1985.

[8] Togai, M. Yamano, O., "Analysis and Design of an Optimal Learning Control Scheme for Industrial Robots: A Discrete System Approach," *Proc. 24th Conf. Decision and Control*, pp. 1399-1404, December 1985.

[9] Atkeson, C.G., Mc.Intyre, J. "Robot Trajectory Learning through Practice," *Proc. IEEE Conf. Robotics and Automation*, pp. 1737-1742, San Francisco, 1986.

[10] Nguyen, C.C., Pooran, F.J., Premack, T., "Learning-Based Hybrid Control of Closed-Kinematic Chain Robotic End-Effectors," *Proc. of 3rd IEEE International Symposium on Intelligent Control*, pp. 545-550 Arlington, Virginia, August 1988.

[11] Nguyen, C.C., Pooran F.J., "Kinematic Analysis and Workspace Determination of a 6 DOF CKCM Robot End-Effector," *Journal of Mechanical Working Technology*, pp. 283-294, June 1989.

[12] Nguyen, C.C., Pooran F.J., "Dynamical Analysis a 6 DOF CKCM Robot End-Effector for Dual-Arm Telerobot Systems," to appear in *Journal of Robotics and Autonomous Systems* , Vol. 5, 1989.

[13] Stewart, D., "A Platform with Six Degrees of Freedom," *Proc. Institute of Mechanical Engineering*, Vol. 180, part 1, No. 5, pp. 371-386, 1965-1966.

[14] Nguyen, C. C., Pooran, F.J. and Premack, T., "Trajectory Control of Robot Manipulator with Closed-Kinematic Chain Mechanism," *Proc. 20th Southeastern Symposium on System Theory*, North Carolina, pp. 454-458, March 1988.

[15] Nguyen, C.C., Pooran, F.J., "Joint-Space Adaptive Control of Robot End-Effectors Performing Slow and Precise Motions," *Proc. 21th Southeastern Symposium on System Theory*, pp. 547-552, Florida, March 1989.

[16] Nguyen, C.C., "Arbitrary Eigenvalue Assignments for Linear Time-Varying Mutltivariable Control Systems,"*International Journal of Control*, Vol. 45, No. 3, pp. 1051-1057, 1987.

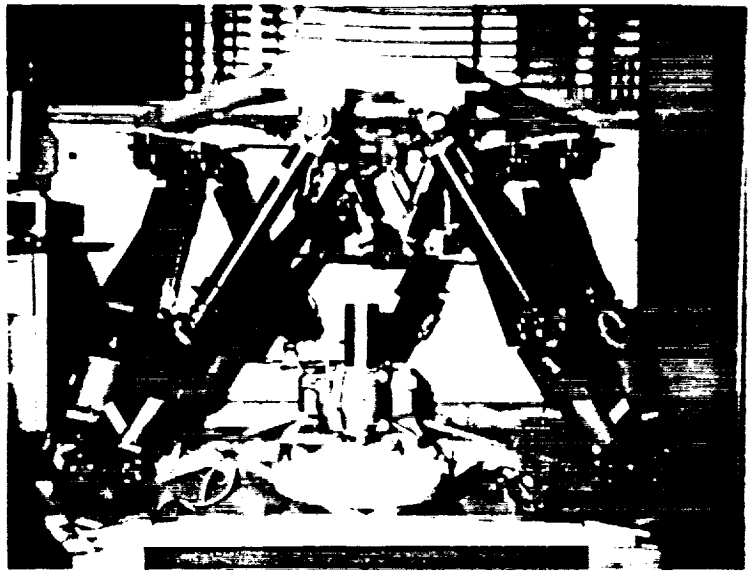

Figure 1: The NASA 6 DOF End-Effector

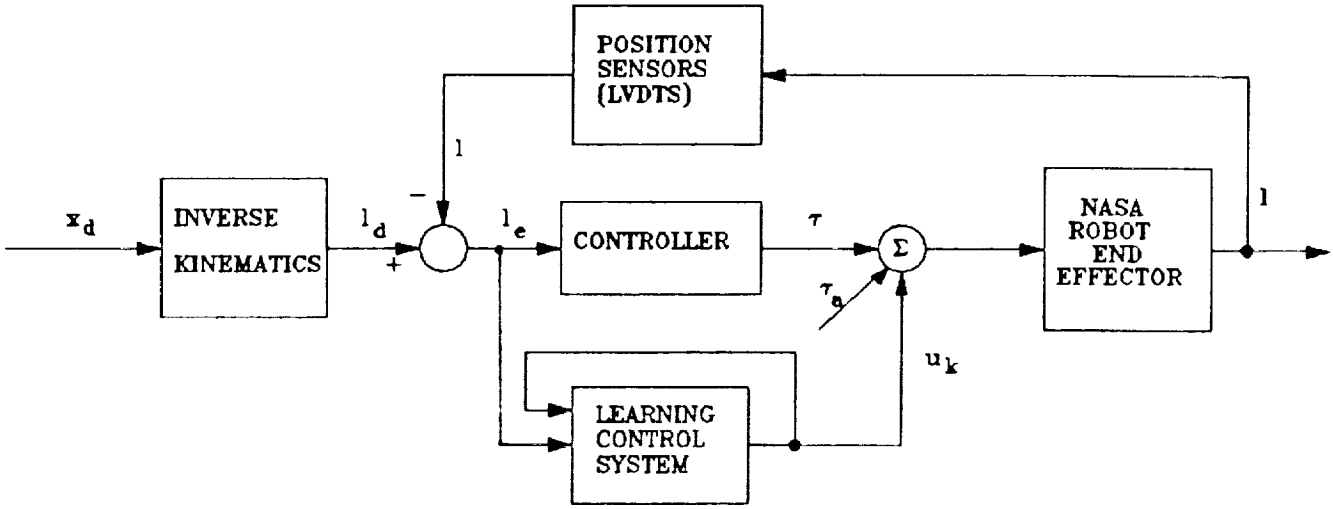

Figure 2: The Learning-Based Control Scheme

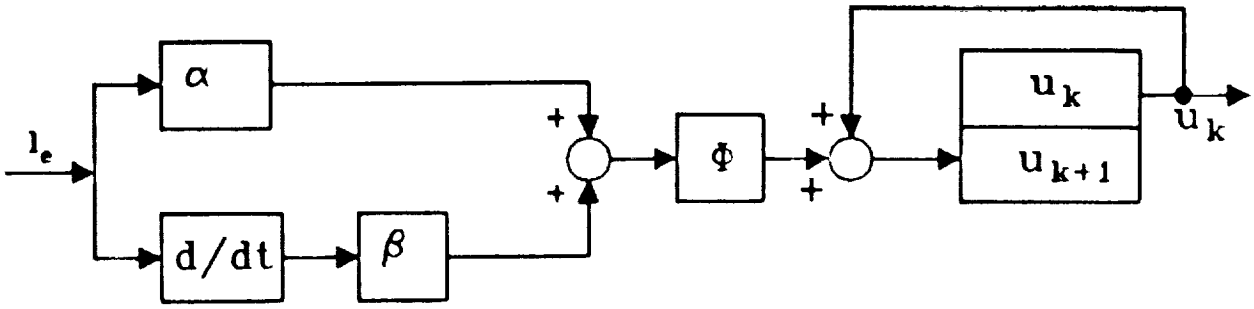

Figure 3: The Learning Controller

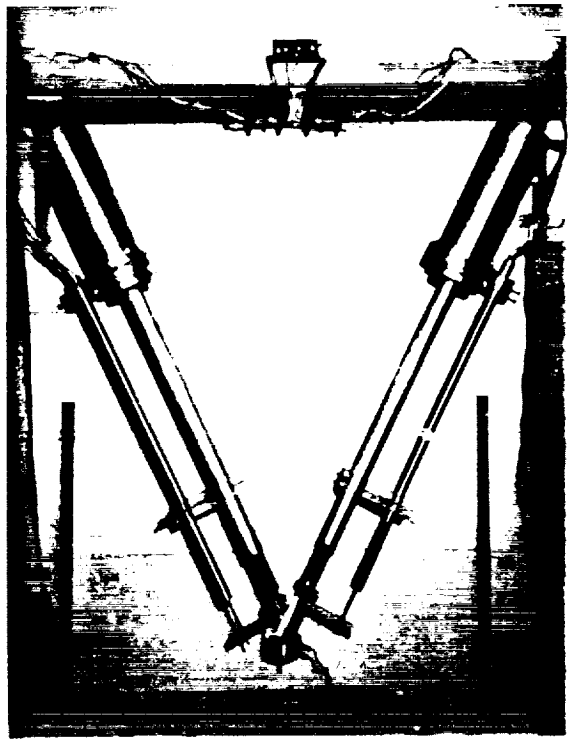

Figure 4: The CUA 2 DOF End-Effector

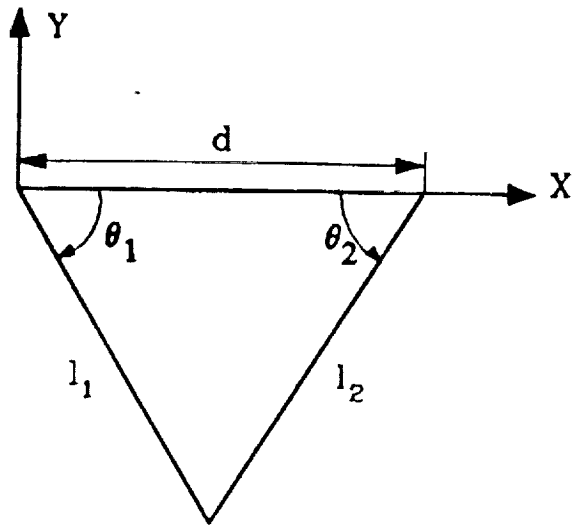

Figure 5: Vector Diagram of the 2 DOF End-Effector

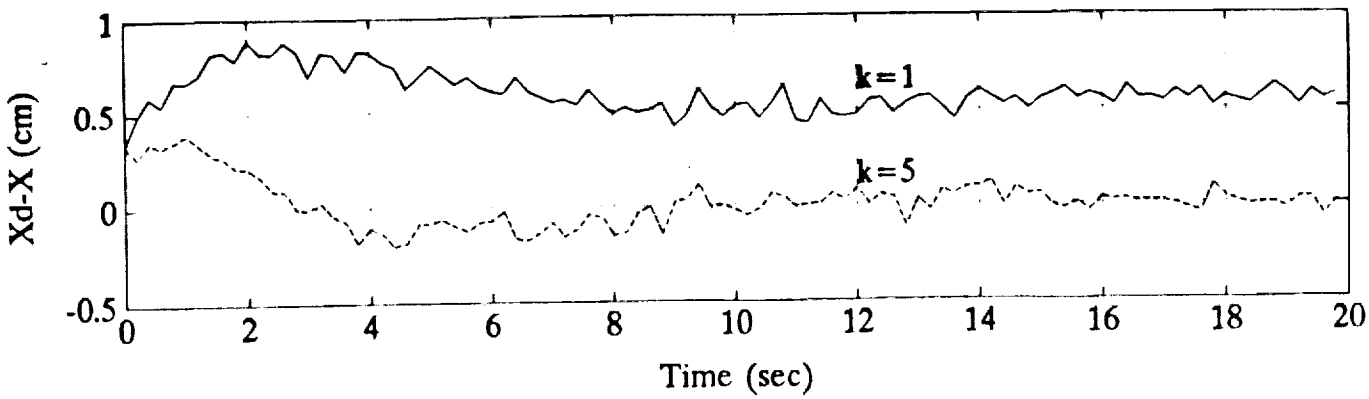

Figure 6-a

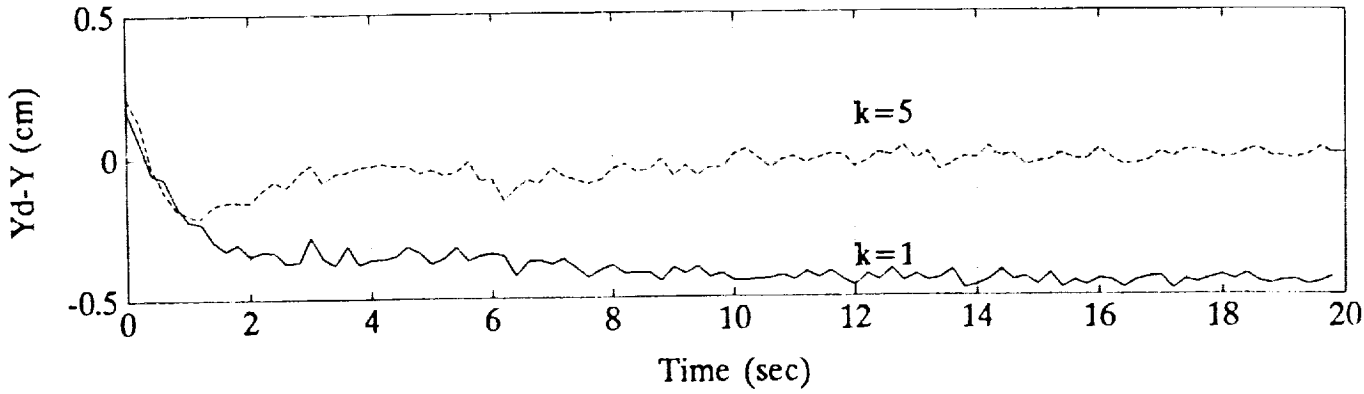

Figure 6-b

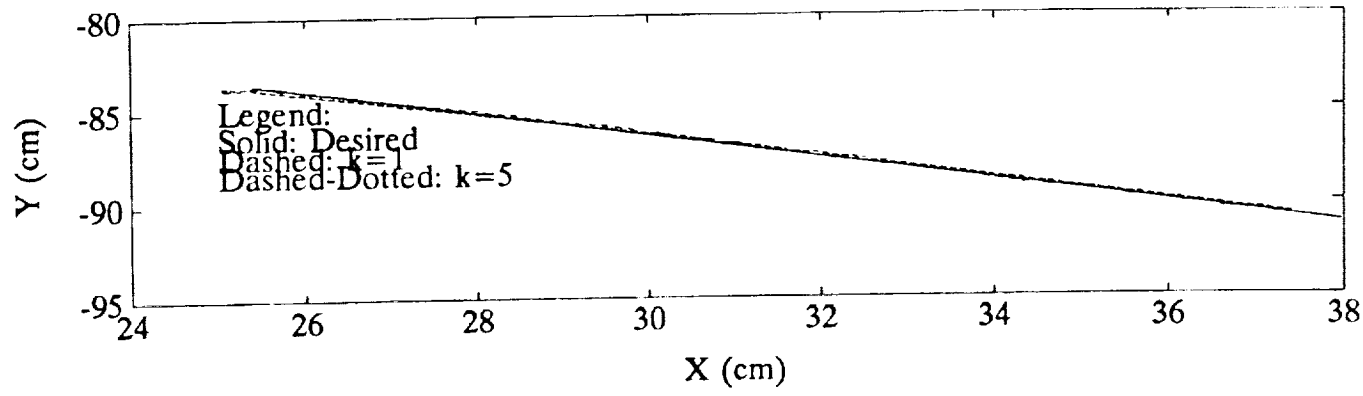

Figure 6-c

Figure 6: Experimental Results of Tracking a Straight Line

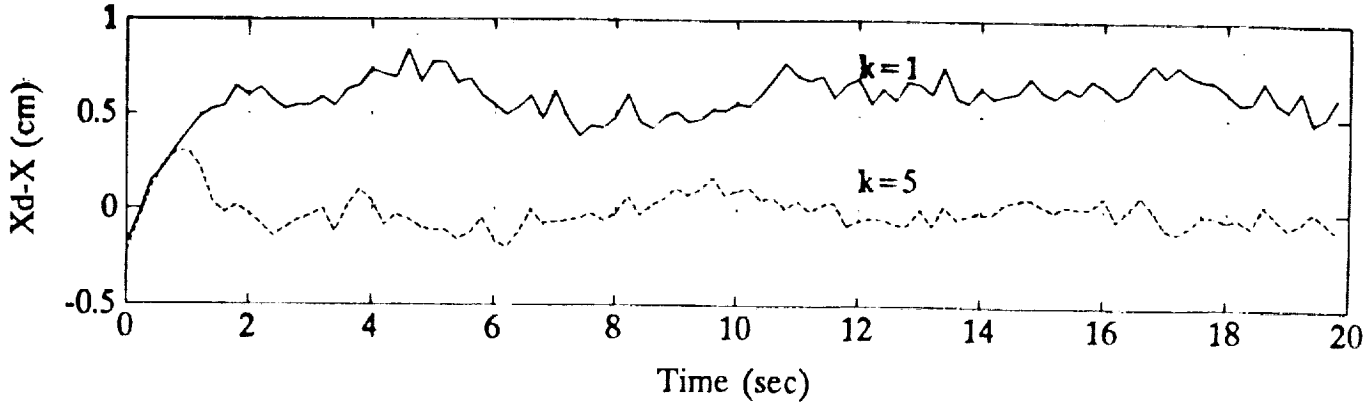

Figure 7-a

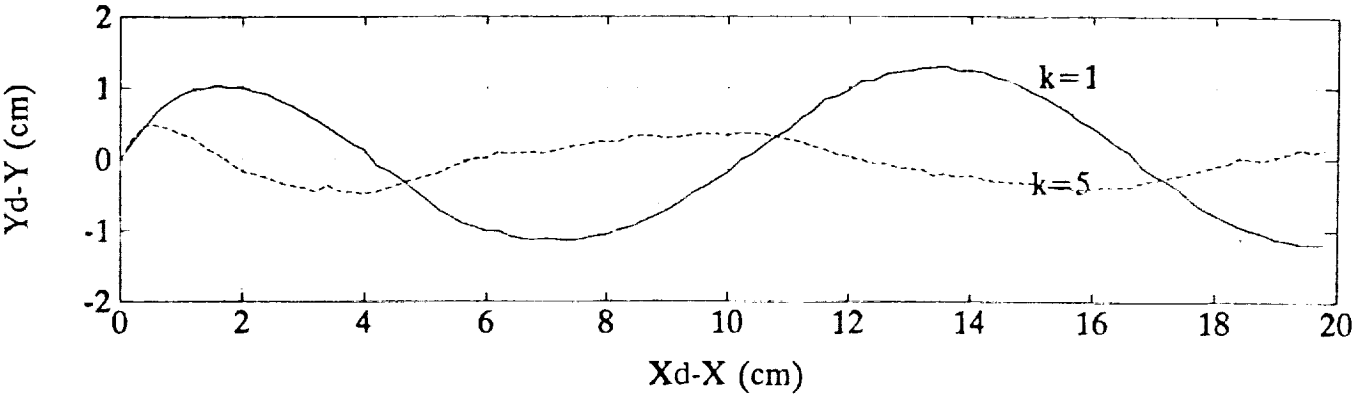

Figure 7-b

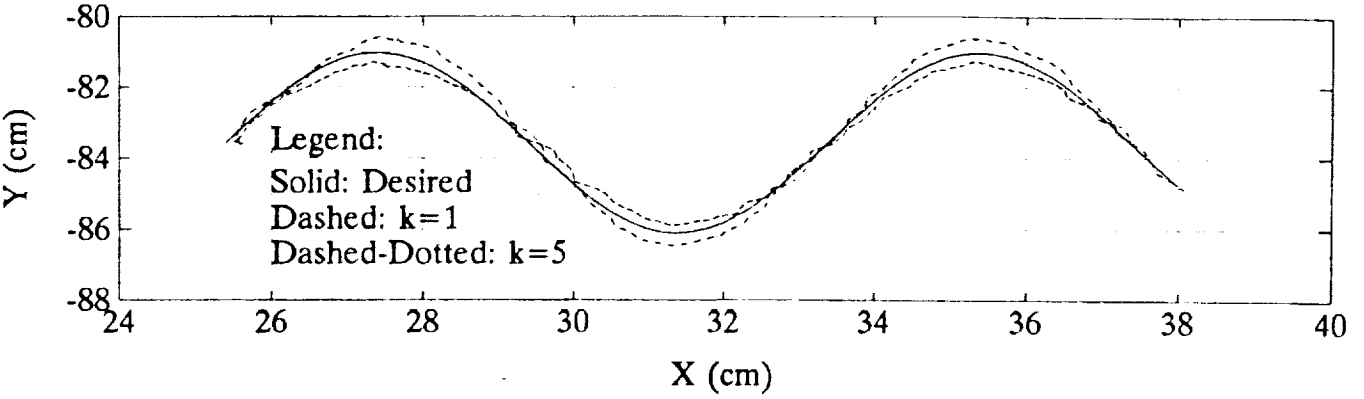

Figure 7-c

Figure 7: Experimental Results of Tracking a Sinusoidal Planar Path

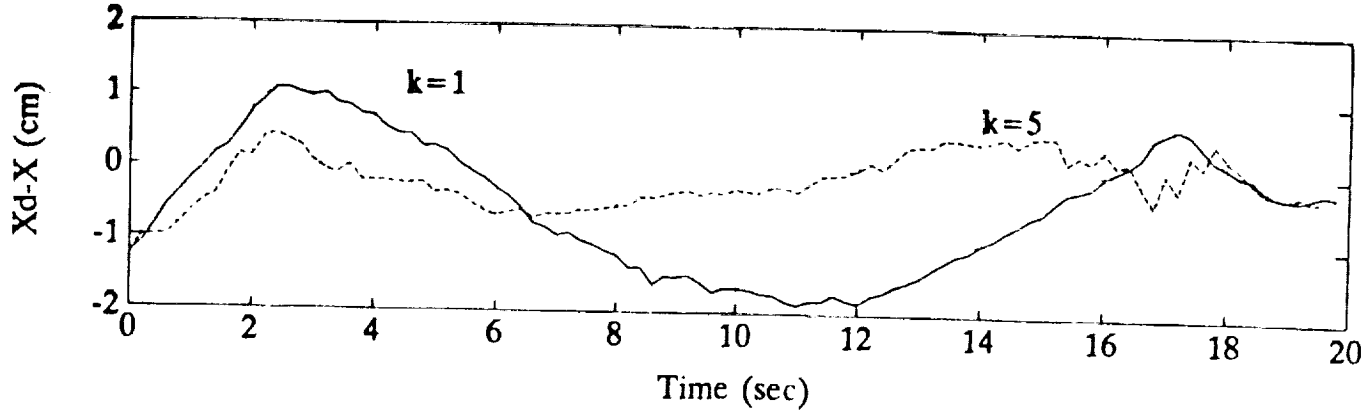

Figure 8-a

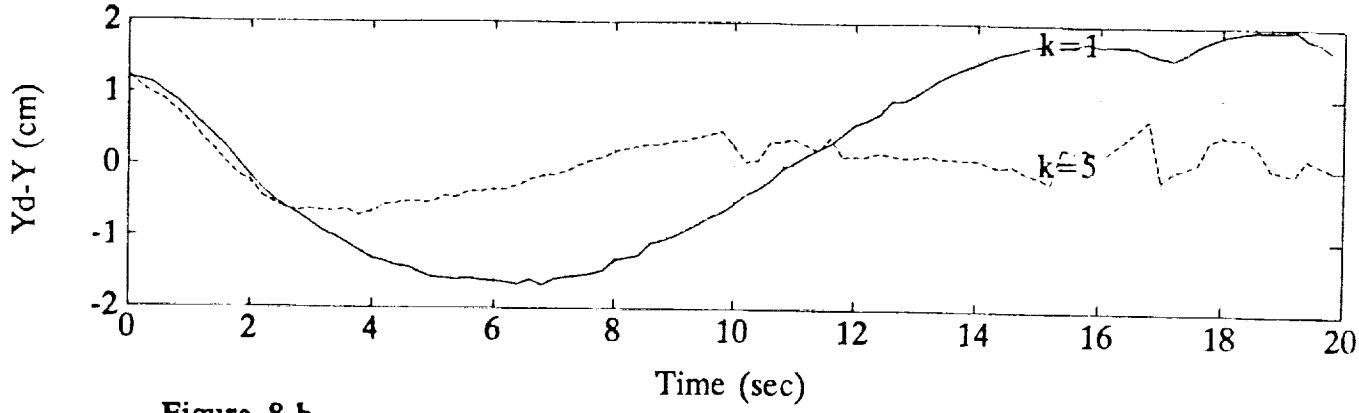

Figure 8-b

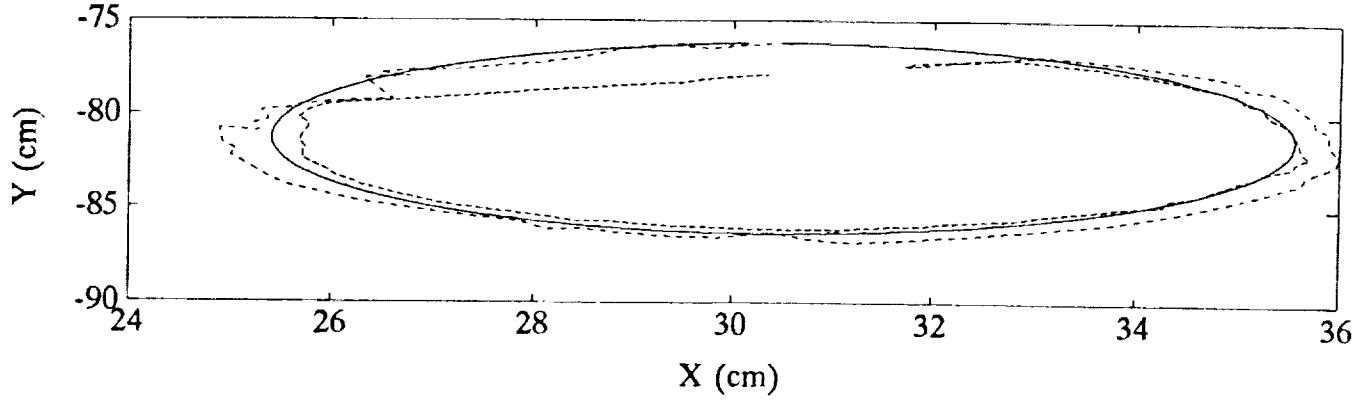

Figure 8-c

Figure 8: Experimental Results of Tracking a Circular Planar Path